

Generalised Sobolev Stable Flux Reconstruction

Will Trojak*

Department of Engineering, University of Cambridge, Cambridge, UK, CB2 1PZ

A new set of correction functions is presented for high-order flux reconstruction, that expands upon, while incorporating, all previous correction function sets and opens the possibility for improved performance. By considering FR applied to the linear advection and modifying the Sobolev norm, the criterion for a wider set of correction functions is presented and sufficient conditions on stability are presented. Legendre polynomials are then used to fulfil these criterion and realise functions for third to fifth order FR. Von Neumann analysis is then applied to analytically find temporal stability limits for various Runge-Kutta temporal integration schemes, and for all cases correction functions are found that extend the temporal stability of FR. Two application-inspired investigations are performed that aim to explore the effect of aliasing and non-linear equations. In both cases unique correction functions could be found that give good performance, compared to previous FR schemes, while also improving upon the temporal stability limit.

I. Introduction

High-order methods have steadily developed over the last half century based on the promise of allowing for complex problems to be tackled both with higher accuracy and greater efficiency. Increased accuracy follows naturally from the increased order and hence low truncation error with higher order scaling. When the application of such methods to Large-Eddy Simulation (LES) is considered, as investigated by Chow¹ and Moin and Ghosal,² high-order becomes key in reducing grid requirements due to the need to reduce aliasing error to a scale such that the sub-grid scale model can effectively characterise unresolved scales. Initially many finite difference methods evolved to harness higher-orders,³ however when moving to complex problems it is beneficial to use unstructured meshes, which becomes particularly difficult in an FD framework.⁴

Reed and Hill⁵ introduced the Discontinuous Galerkin (DG) method which, through its own evolution,⁶ lead to the development of Spectral Volume (SV). Huynh⁷ and later Wang and Goa⁸ introduced a finite element method that built on the developments of SV and DG to form the foundation of what is now Flux Reconstruction (FR). FR is a high order finite element method that uses the propagation of corrections between elements to form a piecewise continuous solution. The character of FR, including the wave propagating performance and temporal integration stability, have been found to be heavily dependent on the manner by which the correction is applied. Several methods emerged for applying the corrections, initially a single parameter family⁹ that incorporated the work of Huynh^{7,10} as well as DG and the Spectral Difference method of Jameson.^{9,11} The same single parameter family was successfully extended for Advection-Diffusion¹² as well for several different multi-dimensional element types.^{13–15} The link between this set of corrections, which will be referred to as Original Stable FR (OSFR), and the mature field of DG was established by Zwanenburg and Nadarajah,¹⁶ together with Mengaldo *et al.*¹⁷ This basis was instrumental in the formation of an extension to the FR correction set, Extended range Stable FR (ESFR).^{18,19}

In this paper a further extension to the correction function set is presented, that aims to incorporate the methods previously presented as well as furthering the potential for improved temporal stability and dispersion and dissipation characteristics. This will be achieved by producing a set of correction functions that is far more general. However, before presenting what will be called Generalised Sobolev Stable FR (GSFR), the current state of the art will be established, this will include the description of OSFR and ESFR. The methodology for deriving GSFR will then be laid out together with the criterion defining the correction function, followed by the criterion on the correction functions necessary for stability. Specific evaluation of the GSFR criterion for several orders will then be presented and the uniqueness of the new functions relative to those of OSFR and ESFR will be proved. To assess the performance of newly presented set, Von Neumann analysis will be utilised to gain insight into the Courant-Freidrichs-Lewy²⁰ (CFL) limits for

the full spatial-temporal discretisation. Lastly a linear heterogeneous equation and Euler's equations will be solved using the GSFR method in order to determine if, when applied to equation sets of significance to engineering, GSFR can give reduced aliasing error and dissipation.

II. Flux Reconstruction

To introduce the numerical underpinning of FR, we begin by considering the 1D scalar conservation law:

$$\frac{\partial u}{\partial t} + \frac{\partial f}{\partial x} = 0 \quad (1)$$

where u is the conserved quantity and $f = f(u)$ is some arbitrary flux function. The spatial domain of the solution will be taken as being Ω , with spatial variable x . This domain can then be divided into sub-domains such that:

$$\Omega = \bigcup_{j=1}^m \Omega_j \quad (2)$$

each of these may be projected onto a regularized reference domain, $\hat{\Omega}$, that is typically taken as being the closed interval $[-1, 1]$ in 1D with reference spatial variable ξ . These definition now allow for the domain to be discretised such that in each sub-domain, Ω_j , there is an ordered set of points $\{x_0, \dots, x_{n_s}\}$. Within the reference domain the discretisation points are the ordered set $\{\xi_0, \dots, \xi_{n_p}\}$. The mapping from sub-domain to reference domain can then be characterised by the Jacobian, J_j , such that the transformed variables are:

$$\hat{u}_j = J_j u_j \quad (3)$$

$$\hat{f}_j = J_j f_j \quad (4)$$

where, for brevity, we are only considering a linear mapping from the physical to reference domain.

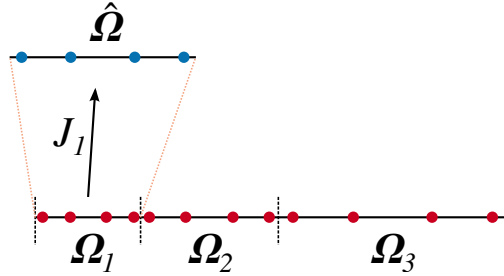


Figure 1: Diagram showing the mapping from the physical domain to the reference domain, with points to show the spatial discretisations.

Within each element a discontinuous polynomial of both the conserved variable and flux variable can then be defined, where \bullet^δ is used to indicate that are variables discontinuous. Hence:

$$\hat{u}^\delta = \sum_{i=0}^p \hat{u}^\delta(\xi_i) l_i(\xi) \quad (5)$$

$$\hat{f}^\delta = \sum_{i=0}^p \hat{f}^\delta(\xi_i) l_i(\xi) \quad (6)$$

where p is the polynomial order and $l_i(\xi)$ are Lagrange polynomial bases in the reference domain, defined as:

$$l_i(\xi) = \prod_{j=0}^p \left(\frac{\xi - \xi_j}{\xi_i - \xi_j} \right) (1 - \delta_{ij}) \quad (7)$$

where δ_{ij} is the Kronecker delta. With this definition, it can be seen that $n_p = p$. In order to form a solution the polynomials defined in the sub-domains must be made to be C^0 continuous, *i.e.* continuous by value between sub-domains. The first step is to find a common flux value at the interface between two

sub-domains based on interpolated values at this interface. The interpolated discontinuous interface values are defined as $\hat{u}^\delta(-1) = \hat{u}_l^\delta$ and $\hat{u}^\delta(1) = \hat{u}_r^\delta$. Many methods are plausible for finding the common interface value, however when solving hyperbolic equations, the upwind direction must be determined by the methods. Therefore, Riemann solvers are appropriate, such as the simple Rusanov approximate Riemann solver²¹ or other two point upwind biased flux calculators (see Toro²²). The notation for the common interface values in a sub-domain is $\hat{f}_{j,l}^I$ and $\hat{f}_{j,r}^I$ for the left and right value respectively in the j^{th} sub-domain. The second

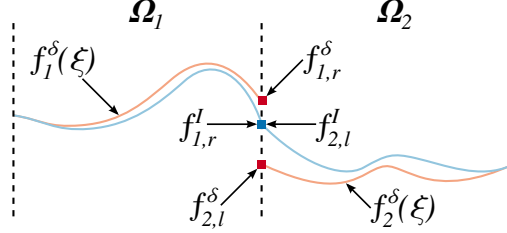


Figure 2: Diagram showing the notation and an interpretation of flux polynomial correction for one interface, cast into the physical domain for simplicity.

step in forming a C^0 continuous solution is to propagate the common interface values into an element. The corrected flux can be broken down into the original discontinuous portion and a correction portion. The flux correction function is formed by scaling a left and right correction, h_l and h_r , function by the difference between the discontinuous and common interface value at the left and right of the cell. Hence, the flux correction can be written as:

$$\hat{f}_j^C(\xi) = (\hat{f}_{j,l}^I - \hat{f}_{j,l}^\delta)h_l(\xi) + (\hat{f}_{j,r}^I - \hat{f}_{j,r}^\delta)h_r(\xi) \quad (8)$$

where the C^0 continuous flux function is then defined as:

$$\hat{f}_j(\xi) = \hat{f}_j^\delta(\xi) + \hat{f}_j^C(\xi) \quad (9)$$

$$= \hat{f}_j^\delta(\xi) + (\hat{f}_{j,l}^I - \hat{f}_{j,l}^\delta)h_l(\xi) + (\hat{f}_{j,r}^I - \hat{f}_{j,r}^\delta)h_r(\xi) \quad (10)$$

The condition that must therefore be imposed on the left and right correction function are then that:

$$h_l(-1) = 1, \quad h_l(1) = 0 \quad (11)$$

$$h_r(-1) = 0, \quad h_r(1) = 1 \quad (12)$$

Equation (10) can then be differentiated and inserted into the linear conservation law of Eq. (1), once the law is projected into the reference domain, thus:

$$\frac{\partial \hat{u}_j}{\partial t} = -\frac{\partial \hat{f}_j}{\partial \xi} \quad (13)$$

$$= -\sum_{i=0}^p \hat{f}_{j,i}^\delta \frac{d l_i(\xi)}{d \xi} - (\hat{f}_{j,l}^I - \hat{f}_{j,l}^\delta) \frac{d h_l(\xi)}{d \xi} - (\hat{f}_{j,r}^I - \hat{f}_{j,r}^\delta) \frac{d h_r(\xi)}{d \xi} \quad (14)$$

At this stage a temporal integration method can be used to advance the solution in time. The result of this integration will once again mean that the conserved variable and flux are discontinuous and hence the correction has to be repeated. The key to the scheme is the definition of the correction function. A set of stable correction functions was first proposed by Vincent *et al.*,⁹ Original Stable FR (OSFR), which is a single parameter set of correction functions. Defined as:

$$h_l = \frac{(-1)^p}{2} \left[\psi_p - \left(\frac{\eta_p \psi_{p-1} + \psi_{p+1}}{1 + \eta_p} \right) \right] \quad (15)$$

$$h_r = \frac{1}{2} \left[\psi_p + \left(\frac{\eta_p \psi_{p-1} + \psi_{p+1}}{1 + \eta_p} \right) \right] \quad (16)$$

$$(17)$$

where:

$$\eta_p = \frac{\iota(2p+1)(a_p p!)^2}{2} \quad (18)$$

$$a_p = \frac{(2p)!}{2^p (p!)^2} \quad (19)$$

and ψ_i is the i^{th} order Legendre polynomials of the first kind defined on $\xi \in [-1, 1]$ with ι taken as a free variable. This set included some previously defined correction functions, such as Huynh's⁷ g_2 scheme, Jameson's¹¹ Spectral Difference scheme or the nodal Discontinuous Galerkin (DG) method. What this also highlights is that the order of the correction function can be $p+1$ and hence the opportunity of additional information being propagated into the sub-domain can be used to increase the order accuracy of the solution.

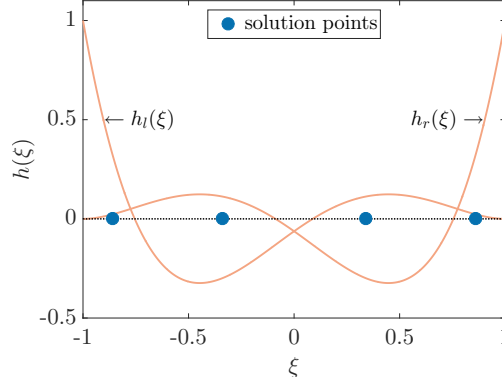


Figure 3: Left and right correction functions for $p = 3$, $\iota = 8/4725$, equivalent to Huynh's g_2 correction function.^{7,9}

Later an extension was made by Vincent *et al.*¹⁸ to give what was called Extended Range Stable FR (ESFR). This set of correction functions was far wider than the of OSFR, with more control variables. To introduce this set of corrections functions we take the gradient of the left correction function to be:

$$\frac{dh_l}{d\xi} = g_l(\xi) = \sum_{i=0}^p \tilde{\mathbf{g}}_i \psi_i(\xi) \quad (20)$$

with the right correction similarly defined, and the notation of $\tilde{\bullet}$ generally used for something either in or cast into a Legendrian basis. It followed that the extended range of correction function was defined by the equations:

$$\tilde{\mathbf{g}}_l = -(\tilde{\mathbf{M}} + \tilde{\mathbf{K}})^{-1} \tilde{\mathbf{l}} \quad (21)$$

$$\tilde{\mathbf{g}}_r = (\tilde{\mathbf{M}} + \tilde{\mathbf{K}})^{-1} \tilde{\mathbf{r}} \quad (22)$$

where $\tilde{\mathbf{l}} = [\psi_0(-1), \dots, \psi_p(-1)]^T$, $\tilde{\mathbf{r}} = [\psi_0(1), \dots, \psi_p(1)]^T$ and

$$\tilde{\mathbf{M}}_{i,j} = \int_{-1}^1 \psi_i \psi_j d\xi = \frac{2}{2j+1} \delta_{i,j}, \quad i, j \in \{0, \dots, p\} \quad (23)$$

Here, $\tilde{\mathbf{K}}$ is a matrix dependent on the free variables $\{\kappa_0, \dots, \kappa_n\}$ where $n = \lfloor p/2 \rfloor + 1$, with some constraints imposed upon $\tilde{\mathbf{K}}$. First, it is necessary to define the following matrices:

$$\mathbf{D}_{i,j} = \frac{dl_j(\xi_i)}{d\xi} \quad (24)$$

$$\mathbf{V}_{i,j} = \psi_j(\xi_i) \quad (25)$$

$$\tilde{\mathbf{D}} = \mathbf{V}^{-1} \mathbf{D} \mathbf{V} \quad (26)$$

Hence, $\tilde{\mathbf{K}}$ is a real matrix satisfying the constraints:

$$\tilde{\mathbf{K}} = \tilde{\mathbf{K}}^T \quad (27)$$

$$\tilde{\mathbf{K}}\tilde{\mathbf{D}} + (\tilde{\mathbf{K}}\tilde{\mathbf{D}})^T = \mathbf{0} \quad (28)$$

$$\tilde{\mathbf{M}} + \tilde{\mathbf{K}} > \mathbf{0} \quad (29)$$

together with $h_l(-1) = h_r(1) = 1$ and $h_l(1) = h_r(-1) = 0$ and symmetry conditions, this defined a multi-parameter set of correction functions, with examples for various orders shown by Vincent *et al.*¹⁸ Further, it was demonstrated that the single parameter OSFR set of Eq.(15 & 16) was a subset of ESFR. To illustrate the correction function set, consider the case of $p = 3$, then, the Legendre coefficients of the correction function gradient can be found to be:

$$\tilde{\mathbf{g}}_1 = - \left[\begin{array}{c} \frac{1}{2} \\ \frac{3(21\kappa_0 + 35\kappa_1 + 6)}{v} \\ \frac{5}{5\kappa_1 + 2} \\ \frac{21(5\kappa_1 + 2)}{v} \end{array} \right] \quad \text{where } v = 175\kappa_1^2 - 42\kappa_0 - 12 \quad (30)$$

III. Generalised Sobolev Stability

In order for a scheme to be stable it is required that the modified broken Sobolev norm exist and be monotonically decreasing with time, properties shown to lead to stability for DG by Hesthaven and Warburton,²³ which was the underpinning of the derivation of OSFR and ESFR. Therefore, we must first define the broken Sobolev norm as:

$$\|u\|_{n,W^{p,2}} = \sqrt{\int_{\Omega_n} \sum_{i=0}^p (u^{(i)})^2 d\xi} \quad (31)$$

where $u^{(i)}$ is the i^{th} spatial derivative of u and $W^{p,2}$ is the p^{th} order l_2 Sobolev space. (In this case $W^{p,2} = H^p$, where H is a Hilbert space). This can then be modified to form:

$$\|u\|_{n,W^{p,2,\iota}} = \sqrt{\int_{\Omega_n} \sum_{i=0}^p \iota_i (u^{(i)})^2 d\xi} \quad (32)$$

where ι_i is a real constant. By inspection it can be seen that this follows the normal rules of norms and hence the metric space is complete in a Cauchy sense. A similar process to this was followed by Vincent *et al.*⁹ however using $\iota_i = 0 \forall 0 < i < p, i \in \mathbb{N}$, which utilises the ability of $|u|_2 + |u^{(p)}|_2$ to sufficiently define a metric and hence infer a topology. However, if the more general version of Eq.(32) is used then there is the potential to find a greater set of metric spaces on the same topology, and hence a more general set of correction functions. The flux reconstructed form of the first order conservation law was introduced in Eq.(14), and if the flux function is set such that linear advection is solved, ($\hat{f}^\delta = \hat{u}^\delta$), then it may be recast as:

$$\frac{\partial \hat{u}^\delta}{\partial t} = - \frac{\partial \hat{u}^\delta}{\partial \xi} - (\hat{u}_l^I - \hat{u}_l^\delta) \frac{dh_l}{d\xi} - (\hat{u}_r^I - \hat{u}_r^\delta) \frac{dh_r}{d\xi} \quad (33)$$

Hence we undertake defining the modified broken Sobolev norm from Eq.(33), which is performed via summation of recursive differentiation and multiplication of the variable. With subsequent integration over the sub-domain to give:

$$\begin{aligned} \frac{1}{2} \frac{d}{dt} \int_{-1}^1 \sum_{i=0}^p \iota_i (\hat{u}^{\delta(i)})^2 d\xi &= - \underbrace{\frac{1}{2} \int_{-1}^1 \sum_{i=0}^p \iota_i \frac{\partial}{\partial \xi} \left(\frac{\partial^i \hat{u}^\delta}{\partial \xi^i} \right)^2 d\xi}_{I_s} - \underbrace{(\hat{u}_l^I - \hat{u}_l^\delta) \int_{-1}^1 \sum_{i=0}^p \iota_i \frac{\partial^i \hat{u}^\delta}{\partial \xi^i} \frac{d^{i+1} h_l}{d\xi^{i+1}} d\xi}_{I_l} \\ &\quad - \underbrace{(\hat{u}_r^I - \hat{u}_r^\delta) \int_{-1}^1 \sum_{i=0}^p \iota_i \frac{\partial^i \hat{u}^\delta}{\partial \xi^i} \frac{d^{i+1} h_r}{d\xi^{i+1}} d\xi}_{I_r} \end{aligned} \quad (34)$$

I_s when combined with one round of integration by parts of I_l and I_r for $i = 0$, is the conservation portion of the equation. Hence, after the integration by parts required to form the conversation integral, the necessary conditions on stability are:

$$\sum_{i=0}^p \iota_i \int_{-1}^1 \frac{d^i h_l}{d\xi^i} \frac{\partial^{i+1} \hat{u}^\delta}{\partial \xi^{i+1}} d\xi = \sum_{i=1}^p \iota_i \left| \frac{\partial^i \hat{u}^\delta}{\partial \xi^i} \frac{d^i h_l}{d\xi^i} \right|_{-1}^1 \quad (35)$$

$$\sum_{i=0}^p \iota_i \int_{-1}^1 \frac{d^i h_r}{d\xi^i} \frac{\partial^{i+1} \hat{u}^\delta}{\partial \xi^{i+1}} d\xi = \sum_{i=1}^p \iota_i \left| \frac{\partial^i \hat{u}^\delta}{\partial \xi^i} \frac{d^i h_r}{d\xi^i} \right|_{-1}^1 \quad (36)$$

If the correction function and solution are taken as being a series of Legendre polynomials:

$$h_l(\xi) = \sum_{i=0}^{p+1} \tilde{\mathbf{h}}_{1i} \psi_i(\xi) \quad \text{and} \quad \hat{u}^\delta(\xi) = \sum_{i=0}^p v_i \psi_i(\xi) \quad (37)$$

then it is possible to find a closed set of equations that define the $h_{l,i}$ in terms of ι_i . Legendre polynomials are chosen as their weighting function for the orthogonality condition is unity, greatly simplifying later derivations. Therefore, substitution of Eq.(37) into Eq.(35) gives:

$$\sum_{i=0}^p \iota_i \int_{-1}^1 \left[\sum_{n=0}^{p+1} \sum_{m=0}^p \tilde{\mathbf{h}}_{1n} v_m \frac{d^i \psi_n}{d\xi^i} \frac{\partial^{i+1} \psi_m}{\partial \xi^{i+1}} \right] d\xi = \sum_{i=1}^p \iota_i \left| \sum_{n=0}^{p+1} \sum_{m=0}^p \tilde{\mathbf{h}}_{1n} v_m \frac{d^i \psi_n}{d\xi^i} \frac{\partial^i \psi_m}{\partial \xi^i} \right|_{-1}^1 \quad (38)$$

The closed set of equations will take the form of:

$$\mathbf{L}_p \tilde{\mathbf{h}}_1 = \begin{bmatrix} 0 & \dots & 0 & 1 \end{bmatrix}^T \quad (39)$$

where the penultimate entries of Eq.(39) are the enforcement of the boundary conditions on h_l , and due to these boundary conditions \mathbf{L}_p , is a square matrix. Exact evaluation of \mathbf{L}_p will follow in Section V

IV. Spatial Validity Limits

In order for the correction function found using the above conditions to be valid, the norm defined by Eq.(32) must be positive and bound, *i.e.* $0 < \|\hat{u}^\delta\|_{n,W^{p,2,\iota}} < \infty$. From the definition of the norm, thus:

$$0 < \int_{-1}^1 \sum_{i=0}^p \iota_i (\hat{u}^{\delta,(i)})^2 d\xi < \infty \quad (40)$$

Then applying Eq.(37):

$$0 < \int_{-1}^1 \sum_{i=0}^p \iota_i \left(\sum_{j=0}^p v_j \frac{\partial^i \psi_j}{\partial \xi^i} \right)^2 d\xi < \infty \quad (41)$$

which can then be simplified to:

$$0 < \sum_{j=0}^p \iota_0 \left(\frac{2}{2j+1} \right) v_j^2 + \int_{-1}^1 \sum_{i=1}^{p-1} \iota_i \left(\sum_{j=0}^p v_j \frac{\partial^i \psi_j}{\partial \xi^i} \right)^2 d\xi + \iota_p \left(\frac{(2p)!}{2^p p!} \right)^2 v_p^2 < \infty \quad (42)$$

A closed form for the value of the product of arbitrary Legendre polynomials is particularly complex, see Bailey²⁴ and Dougall,²⁵ hence numerical evaluation can be used and will be laid out in Section V

V. Generalised Sobolev Correction Functions

In the previous sections the conditions for stability of FR and the limits on the ranges of $\mathbf{I}_p = [\iota_0 \dots \iota_p]^T$ were discussed. However, the presented generalised form is quite abstract and so this section will present

some specific evaluated cases. If we start by writing that the general form of the entries of \mathbf{L}_p can be written as:

$$\mathbf{L}_p[m-1][n] = \sum_{i=0}^p \iota_i \int_{-1}^1 \frac{d^i \psi_n}{d\xi^i} \frac{d^{i+1} \psi_m}{d\xi^{i+1}} d\xi - \sum_{i=1}^p \iota_i \left[\frac{d^i \psi_n}{d\xi^i} \frac{d^i \psi_m}{d\xi^i} \right]_{-1}^1 \quad (43)$$

where $m, n \in \mathbb{N}$ with $1 \leq m \leq p$ and $0 \leq n \leq p$. The $m = 0$ case is removed as it is identically zero, and the final two rows will come from the boundary conditions on $h_i(\xi)$. To evaluate Eq.(43), it can be useful to consider the following result of Miller,²⁶ which we modified to consider Legendre polynomials and the prescribed relationship of the derivatives.

$$\int_{-1}^1 \frac{d^m \psi_n}{d\xi^m} \frac{d^{m+1} \psi_k}{d\xi^{m+1}} d\xi = \sum_{i=0}^{\lfloor \frac{n-m}{2} \rfloor} \sum_{j=0}^{\lfloor \frac{k-m-1}{2} \rfloor} \frac{b_i(m, n) b_j(m+1, k)}{n+k-2(m+i+j)} [1 - (-1)^{n+k-2(m+i+j)}] \quad (44)$$

where we define:

$$b_i(m, n) = \frac{(-1)^i (2(n-i))!}{2^n (n-m-2i)! (n-i)! i!} \quad (45)$$

Then for the gradient of Legendre polynomials at the end point:

$$\frac{\partial^n \psi_j(-1)}{\partial \xi^n} = \frac{(-1)^{j-n} (j+n)!}{2^n n! (j-n)!} \quad \text{and} \quad \frac{\partial^n \psi_j(1)}{\partial \xi^n} = \frac{(1)^{j-n} (j+n)!}{2^n n! (j-n)!} \quad \text{for } j \geq n \quad (46)$$

which can be inferred from the work of Garfinkel²⁷ and Holdeman.²⁸ With these identities established specific examples may now be evaluated.

V.A. GSFR for $p = 2$

For the case of $p = 2$ the generalised correction function equation can be found to be:

$$\mathbf{L}_2 \tilde{\mathbf{h}}_1 = \begin{bmatrix} -\iota_0 & 0 & 3\iota_1 & 0 \\ 0 & -\iota_0 & 0 & 15(\iota_1 + 3\iota_2) \\ 1 & 1 & 1 & 1 \\ 1 & -1 & 1 & -1 \end{bmatrix} \tilde{\mathbf{h}}_1 = \begin{bmatrix} 0 \\ 0 \\ 0 \\ 1 \end{bmatrix} \quad (47)$$

And upon assessment of the limits presented by Eq.(42), the limits on \mathbf{I}_2 can be found to be:

$$\begin{bmatrix} 0 \\ -\frac{1}{2} \left(\frac{2}{3} \iota_0 \right) \\ -\frac{1}{3} \left(\frac{2}{5} \iota_0 + 6\iota_1 \right) \end{bmatrix} < \mathbf{I}_2 < \infty \quad (48)$$

V.B. GSFR for $p = 3$

$$\begin{bmatrix} -\iota_0 & 0 & 3\iota_1 & 0 & 10\iota_1 \\ 0 & -\iota_0 & 0 & 15(\iota_1 + 3\iota_2) & 0 \\ -\iota_0 & 0 & -(\iota_0 - 3\iota_1) & 0 & 15(3\iota_1 + 35\iota_2 + 105\iota_3) \\ 1 & 1 & 1 & 1 & 1 \\ 1 & -1 & 1 & -1 & 1 \end{bmatrix} \tilde{\mathbf{h}}_1 = \begin{bmatrix} 0 \\ 0 \\ 0 \\ 0 \\ 1 \end{bmatrix} \quad (49)$$

Evaluating Eq.(42), the condition necessary for valid correction functions is:

$$0 < 2\iota_0 v_0^2 + \left(\frac{2}{3} \iota_0 + \iota_1 \right) v_1^2 + \left(\frac{2}{5} \iota_0 + 6\iota_1 + 18\iota_2 \right) v_2^2 + \left(\frac{2}{7} \iota_0 + 8\iota_1 + 150\iota_2 + 255\iota_3 \right) v_3^2 + \iota_1 (v_1 + 2v_3)^2 < \infty \quad (50)$$

Due to the final term in Eq.(50), the transformation of this to a necessary condition on \mathbf{I}_3 is difficult. However, it can lead to a sufficient condition on the range of validity for \mathbf{I}_3 :

$$\begin{bmatrix} 0 \\ 0 \\ -\frac{1}{18}\left(\frac{2}{5}\iota_0 + 6\iota_1\right) \\ -\frac{1}{255}\left(\frac{2}{7}\iota_0 + 8\iota_1 + 150\iota_2\right) \end{bmatrix} < \mathbf{I}_3 < \infty \quad (51)$$

V.C. GSFR for $p = 4$

$$\begin{bmatrix} \iota_0 & 0 & 3\iota_1 & 0 & 10\iota_1 & 0 \\ 0 & \iota_0 & 0 & 15(\iota_1 + 3\iota_2) & 0 & (42\iota_1 + 315\iota_2) \\ \iota_0 & 0 & (\iota_0 + 3\iota_1) & 0 & 15(3\iota_1 + 35\iota_2 + 105\iota_3) & 0 \\ 0 & \iota_0 & 0 & (-\iota_0 + 15\iota_1 + 150\iota_2) & 0 & 105(\iota_1 + 31\iota_2 - 63\iota_3 + 945\iota_4) \\ 1 & 1 & 1 & 1 & 1 & 1 \\ 1 & -1 & 1 & -1 & 1 & -1 \end{bmatrix} \tilde{\mathbf{h}}_1 = \begin{bmatrix} 0 \\ 0 \\ 0 \\ 0 \\ 0 \\ 1 \end{bmatrix} \quad (52)$$

Evaluating Eq.(42) to find the necessary limits on validity:

$$\begin{aligned} 0 < 2\iota_0 v_0^2 + \left(\frac{2}{3}\iota_0 + \iota_1\right)v_1^2 + \left(\frac{2}{5}\iota_0 + 2\iota_1 + 9\iota_2\right)v_2^2 + \left(\frac{2}{7}\iota_0 + 8\iota_1 + 150\iota_2 + 450\iota_3\right)v_3^2 \\ + \left(\frac{2}{9}\iota_0 + 11\iota_1 + 290\iota_2 + 7350\iota_3 + 11025\iota_4\right)v_4^2 \\ + \iota_1(2v_2 + 3v_4)^2 + \iota_1(v_1 + 2v_3)^2 + \iota_2(3v_2 + 20v_4)^2 < \infty \end{aligned} \quad (53)$$

And hence, with the same reasoning as for $p = 3$, the sufficient conditions on \mathbf{I}_4 for valid correction functions are:

$$\begin{bmatrix} 0 \\ 0 \\ 0 \\ -\frac{1}{450}\left(\frac{2}{7}\iota_0 + 8\iota_1 + 150\iota_2\right) \\ -\frac{1}{105^2}\left(\frac{2}{9}\iota_0 + 11\iota_1 + 290\iota_2 + 7350\iota_3\right) \end{bmatrix} < \mathbf{I}_4 < \infty \quad (54)$$

At this point it is worth noting the recursive nature of the matrix \mathbf{L}_p . Hence the set of correction functions at p is the union of p^{th} order correction functions and the correction functions defined by \mathbf{L}_{p-1} and so on recursively down to the empty set. So if the p^{th} order correction function is defined by some eigenfunction \mathbf{c}_p then the space of correction functions is defined as $\oplus_{i=0}^p \mathbf{c}_i$, *i.e* each time the order is increased, one extra eigenfunction is introduced. However, in the special case of $\mathbf{I}_p = [1, 0, \dots]^T$, the set of correction functions collapse to a single value, unique for each p . This is an interesting property that will be explored in future work.

To show that these correction functions are in fact unique by comparison to both the OSFR of Vincent *et al.*⁹ and the ESFR of Vincent *et al.*,¹⁸ an attempt must be made to reconstruct the GSFR correction functions in both the ESFR and the OSFR setting. Starting with OSFR, this method defines only the free parameter ι , as described in Eq.(15 & 18). Taking $p = 3$ and defining some arbitrary stable value of \mathbf{I}_3 , the equivalent value of ι can be found using the value of $\tilde{\mathbf{h}}_{p+1}$ found from Eq.(49). Hence:

$$\iota = \frac{1}{(2p+1)(a_p p!)^2} \left(\frac{(-1)^{p+1}}{\tilde{\mathbf{h}}_{p+1}} - 2 \right) \quad (55)$$

To then compare to ESFR, it is easier to consider the gradient of h_l , defined in Eq.(20), and defining the Legendre polynomial weights of GSFR similarly as $\tilde{\mathbf{g}}_l$. Then for the case of $p = 3$ the corresponding ESFR

weights can be found, using Eq.(30) from Vincent *et al.*,¹⁸ as:

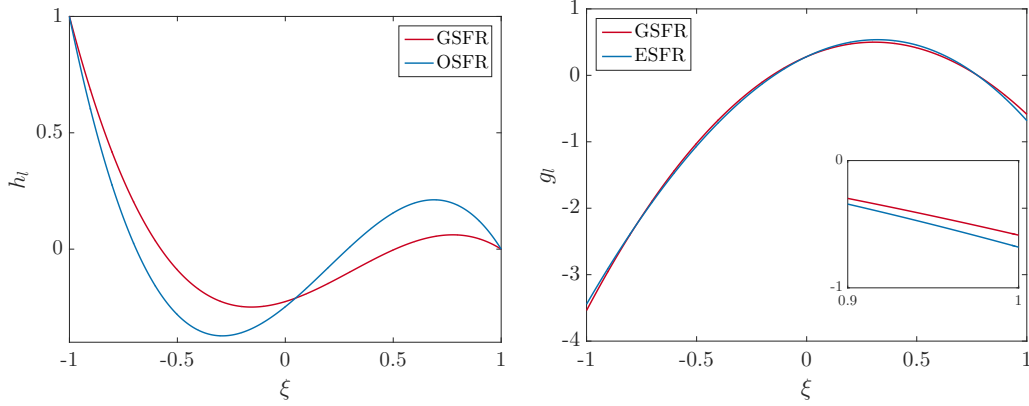
$$\kappa_1 = -\left(\frac{1}{\tilde{\mathbf{g}}_{12}} + \frac{2}{5}\right) \quad (56)$$

$$\kappa_0 = \frac{175\kappa_1^2\tilde{\mathbf{g}}_{11} + 105\kappa_1 - 12\tilde{\mathbf{g}}_{11} + 18}{42\tilde{\mathbf{g}}_{11} - 63} \quad (57)$$

It can then be further shown that to be an ESFR correction function for $p = 3$, together with Eq.(56), the following must be satisfied:

$$\frac{175\kappa_1^2\tilde{\mathbf{g}}_{13} + 105\kappa_1 + 42 - 12\tilde{\mathbf{g}}_{13}}{42\tilde{\mathbf{g}}_{13}} = \frac{175\kappa_1^2\tilde{\mathbf{g}}_{11} + 105\kappa_1 - 12\tilde{\mathbf{g}}_{11} + 18}{42\tilde{\mathbf{g}}_{11} - 63} \quad (58)$$

where κ_1 is defined by Eq.(56). As is shown in Fig. 4 the correction functions found by satisfying Eq.(35 & 36)



(a) Left correction function comparison between OSFR and GSFR (b) Left correction function gradient comparison between ESFR and GSFR.

Figure 4: Comparison of OS, ES and GS correction functions. For $p = 3$ and taking $\mathbf{I}_3 = [1, 0.01, 0.01, 0.1]^T$

are in fact different from those defined by OSFR and ESFR. Furthermore, for OSFR it is trivial to show that it is a sub-set of GSFR, from there respective definitions, OSFR can be constructed when $\mathbf{I}_p = [1, \dots, 0.5\iota]^T$. The ESFR norm definition detailed in¹⁸ can be used to show ESFR is a subset of GSFR. This result could be expected as both OSFR and ESFR were found to be Sobolev stable. To find the corresponding values of \mathbf{I}_p for a given h_l , originating from either OSFR or ESFR, the subject of the equation defining the GSFR correction must be change to \mathbf{I}_p . In the case of $p = 3$ and setting $\iota_0 = 1$, this takes the form:

$$\underbrace{\begin{bmatrix} 3\tilde{\mathbf{h}}_{12} + 10\tilde{\mathbf{h}}_{14} & 0 & 0 \\ 15\tilde{\mathbf{h}}_{13} & 45\tilde{\mathbf{h}}_{13} & 0 \\ 3\tilde{\mathbf{h}}_{12} + 45\tilde{\mathbf{h}}_{14} & 525\tilde{\mathbf{h}}_{14} & 1575\tilde{\mathbf{h}}_{14} \end{bmatrix}}_{\mathbf{H}_3} \begin{bmatrix} \iota_1 \\ \iota_2 \\ \iota_3 \end{bmatrix} = \begin{bmatrix} \tilde{\mathbf{h}}_{10} \\ \tilde{\mathbf{h}}_{11} \\ \tilde{\mathbf{h}}_{10} + \tilde{\mathbf{h}}_{12} \end{bmatrix} \quad (59)$$

Hence, ESFR and OSFR are both recoverable from GSFR. The exception to the invertibility of \mathbf{H}_3 over the set of ESFR and OSFR is when either $\tilde{\mathbf{h}}_{13} = 0$ or $\tilde{\mathbf{h}}_{14} = 0$, as GSFR has multiple ways of constructing these lower order correction functions.

VI. Von Neumann Analysis

Initial characterisation of the set of schemes defined by the GSFR correction functions is investigated via von Neumann analysis applied to the linear advection equation. With unit wave speed, this can be cast as the semi-discrete matrix equation for flux reconstruction:

$$\frac{\partial \mathbf{u}_j}{\partial t} = -\left(J_{j+1}^{-1} \mathbf{C}_{+1} \mathbf{u}_{j+1} + J_j^{-1} \mathbf{C}_0 \mathbf{u}_j + J_{j-1}^{-1} \mathbf{C}_{-1} \mathbf{u}_{j-1}\right) \quad (60)$$

where J_j is the j^{th} element's Jacobian and defining the operator matrices as:

$$\mathbf{C}_{+1} = (1 - \alpha)\mathbf{g}_r\mathbf{l}_l^T \quad (61)$$

$$\mathbf{C}_0 = \mathbf{D} - \alpha\mathbf{g}_l\mathbf{l}_l^T - (1 - \alpha)\mathbf{g}_r\mathbf{l}_r^T \quad (62)$$

$$\mathbf{C}_{-1} = \alpha\mathbf{g}_l\mathbf{l}_r^T \quad (63)$$

where α is the upwinding ratio, \mathbf{g}_l is the value of $g_l(\xi)$ at the solution quadrature points and \mathbf{l}_l is a vector interpolating from the solution points to the left interface. With \mathbf{g}_r and \mathbf{l}_r similarly defined. This method was initially presented by Trojak *et al.*²⁹ and is similar to that of Vincent *et al.*³⁰ If a Bloch wave is then defined such that:

$$u(x, t) = v \exp(i(kx - \omega t)) \quad (64)$$

then the discretised equation can be found to be:

$$\frac{\partial \mathbf{u}_j}{\partial t} = -\left(J_{j+1}^{-1}\mathbf{C}_{+1} \exp(-ik\delta_j) + J_j^{-1}\mathbf{C}_0 + J_{j-1}^{-1}\mathbf{C}_{-1} \exp(-ik\delta_{j-1})\right)\bar{\mathbf{u}}_j = \mathbf{Q}(k)\bar{\mathbf{u}}_j \quad (65)$$

where $\delta_j = x_j - x_{j-1}$. Therefore, after differentiating the Bloch wave w.r.t. time, the wave phase velocity can be found from the eigenvalue problem:

$$c(k)\mathbf{v} = \frac{i}{k}\mathbf{Q}(k)\mathbf{v} \quad (66)$$

Therefore, the dispersion and dissipation can be found as $\Re(\hat{\omega}) = \Re(c)\hat{k}$ and $\Im(\hat{\omega}) = \Im(c)\hat{k}$ respectively. To investigate the fully-discretised equation, a temporal discretisation can be included by defining the fully-discretised linear operator, or update matrix, as:

$$\mathbf{u}_j^{n+1} = \mathbf{R}(\mathbf{Q})\mathbf{u}_j^n \quad (67)$$

$$\mathbf{R}_{44} = \sum_{n=0}^4 \frac{(\tau\mathbf{Q})^n}{n!} \quad (68)$$

where τ is the explicit time integration step and \mathbf{R}_{44} gives an example definition of the update matrix for RK44 temporal integration. Therefore, for von Neumann type spatial-temporal stability to be assured,³¹ the spectral radius of the update matrix must be less than or equal to 1, $\rho(\mathbf{R}) \leq 1$.

VI.A. Results

As was discussed in Section V, the cross product between some of the solution weights, for example the last term in Eq.(50), leads to difficulty in transforming the necessary condition for a positive definite norm to a condition on \mathbf{I}_p . Although a sufficient condition on \mathbf{I}_p can be found, \mathbf{I}_p will be allowed to vary beyond these bounds to aid understanding in the underlying necessary condition. Throughout this analysis ι_0 will also be taken as one; it should be understood that this is an arbitrary choice, but that choosing a different value will simply lead to a linear scaling of all other ι_i values shown here.

Beginning with the case of $p = 3$, Fig. 5 shows the variation of CFL number with \mathbf{I}_3 for low storage RK44 temporal integration. In this figure positive and negative log axes in ι_2 and ι_3 are used to clearly show the CFL manifold, the join is at $\pm 10^{-5}$. This chiefly shows the extent of the domain of \mathbf{I}_3 and also highlights some regions of interest. The first region to consider is that as $\iota_3, \iota_2 \rightarrow \infty$, in this case the correction function converges upon $p = 2$ correction functions. This is similar to the properties of the ESFR scheme. Secondly, in Fig.5a, a region at $\iota_1 = 5 \times 10^{-2}$ as $\iota_2 \rightarrow \infty$. Here an almost one dimensional region of high CFL is present, where the correction function order drops further to $p = 1$. Lastly consider the region where $\mathbf{I}_3 \approx [1, 0, 10^{-3}, 10^{-3}]^T$, here the CFL limit can be seen to have a local maximum. This region of local maximum is believed to give recovery of high-order due to the scale of the Legendre weights, which can be shown analytically through the position of the Nyquist wavenumber of the semi-discretised form, with degradation in the Nyquist limit indicating a drop in order of accuracy (OOA). To exactly find the OOA a numerical method will be introduced in Section VII.

The investigation of the dispersion and dissipation for some selected correction functions when $p = 3$ is presented in Fig.6. The third correction function tested is that which gives peak CFL performance. In

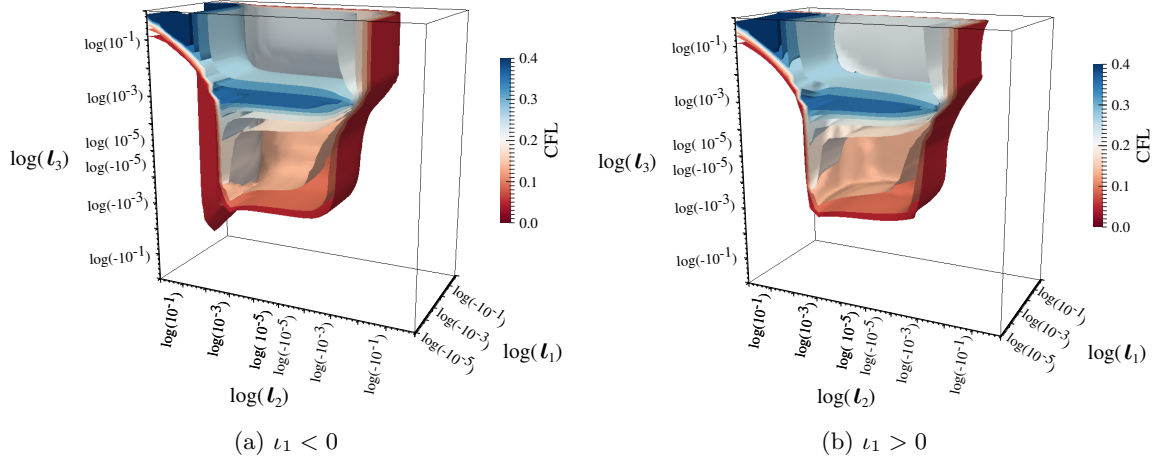


Figure 5: CFL limit for upwinded FR with GSFR correction functions, $p = 3$, and RK44 temporal integration on a regular grid.

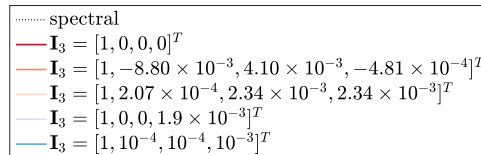
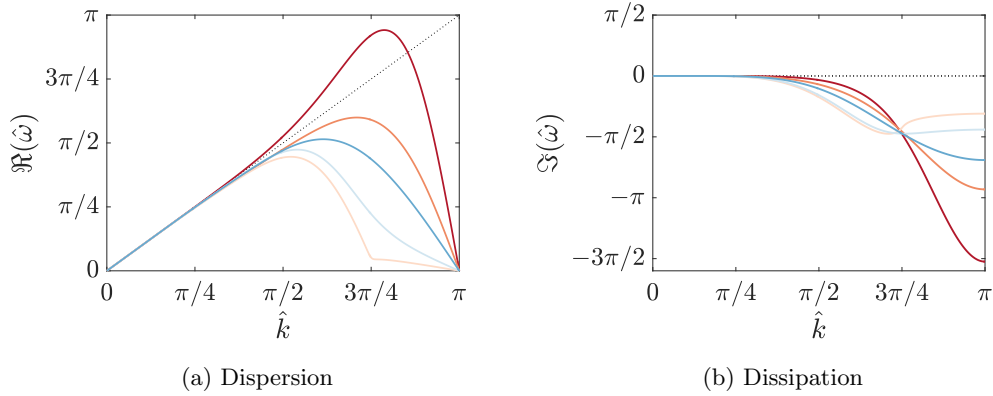


Figure 6: Dispersion and dissipation for selected $p = 3$ GSFR correction functions with interface upwinding.

this case the Nyquist wavenumber is maintained at that for an OOA of four. However, a drop in the phase velocity, $c_p = \omega/k$, at high wavenumber is exhibited, but associated with this there has been a significant reduction in the dissipation. The combination of these has then given rise to an increased CFL limit, but at the cost of spectral performance.

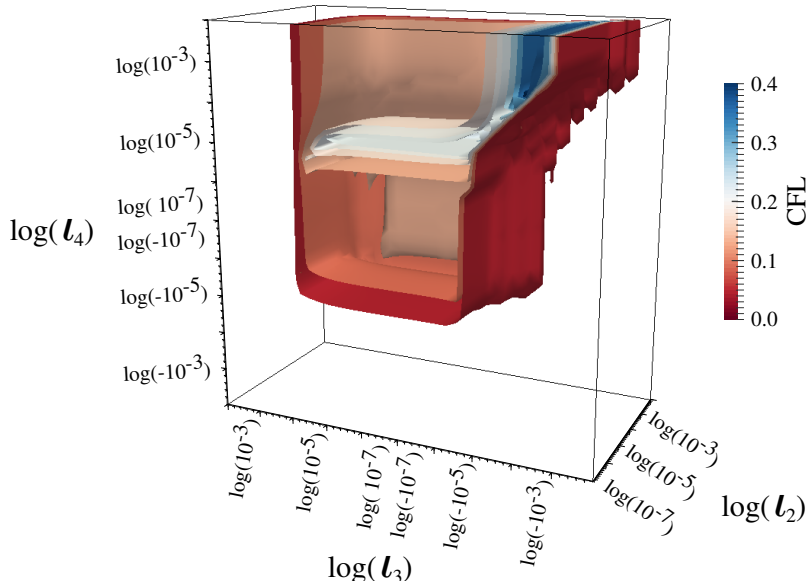


Figure 7: CFL limit for upwinded FR with GSFR correction functions, $p = 4$, and RK44 temporal integration on a regular grid. ($\iota_1 = 1 \times 10^{-5}$)

Returning to the investigation of CFL limits, Fig. 7 shows two regions of interest for $p = 4$ which are similar to those shown for $p = 3$. However, now with the first region found in $-\iota_3$ half plan, which may have been predicted by the interaction of the odd and even powers. Although a localised maximum CFL limit can be seen, the free parameter is four dimensional, and hence a search method will have to be used to find the global high-order recovering maximum CFL limit. This method will be introduced in Section VII.

VII. Numerical Tests

Numerical tests were undertaken to validate analytical findings and provide useful further insight. The first such numerical test was contrived to calculate the OOA of the scheme while solving the linear advection equation with wave speed of unity. The domain set-up for this case was a periodic domain with $x \in [0, 2\pi]$, with the number of elements allowed to vary such that varying degrees of freedom could be tested. The interfaces were fully upwinded and a time step was chosen such that the temporal integration was not the primary source of error. The initial solution was taken to be a plane wave, with a wavenumber that would be expected to be well resolved on the grids:

$$u(x; t = 0) = u^e(x; t = 0) = \cos(kx), \quad k = \frac{1}{2\pi} \quad (69)$$

where $u^e(x, t)$ is the exact solution and $u(x, t)$ is the approximate solution from FR. Taking the solution after some number of time integrations, the point averaged error can be calculated for several grid densities, with n_s points:

$$\epsilon_2 = \frac{1}{n_s} \sum_{i=1}^{n_s} |u^e(x_i, t) - u(x_i, t)| \quad (70)$$

$$\epsilon_2 = |u^e(x, t) - u(x, t)| = \mathcal{O}(n_s^{-k}) \quad (71)$$

where k is the numerically realised OOA, which can be found through taking logs of Eq.(71). With this established, the correction functions can now be varied to show the effect of \mathbf{I}_p on OOA.

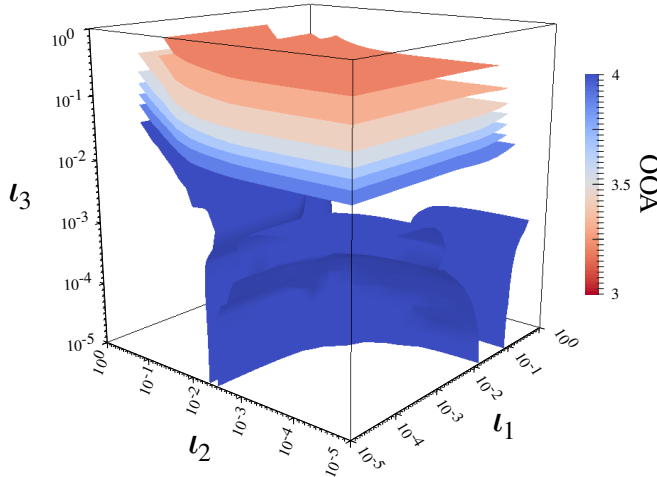


Figure 8: Order of accuracy of GSFR, $p = 3$ for linear advection of a wave with $k = 1/2\pi$, at $t = \pi$.

Figure 8 shows one of the regions of interest for the case of $p = 3$. What can be noted is that the analytically predicted decrease in order as $\iota_3 \rightarrow \infty$ is demonstrated numerically, with $\text{OOA} \rightarrow p$. Reassuringly, the order accuracy in the region of $\iota_3 \approx 10^{-3}$, where peak temporal stability is believed to lie, is shown to have $\text{OOA} = p + 1$ and hence the maximum CFL limit may be increased without an apparent loss in order accuracy. It may, therefore, be productive to perform a search of correction functions, in order to find the peak CLF limit. The domain of \mathbf{I}_p is sufficiently small, permitting an exhaustive search that couples the numerical OOA calculation and analytic CFL calculation to find the maximum CFL limit. The results of this search are shown in Table 1, in all cases the OOA recovered was $p + 1$, consistent with the expected order. It may be noted that in some cases a significant improvement upon the CFL limit may be made by comparison to Vincent *et al.*³⁰

Table 1: Peak CFL of Order recovering GSFR

p	RK Scheme	\mathbf{I}_p	τ
3	RK33	$[1, 1.274 \times 10^{-3}, 1.438 \times 10^{-2}, 7.848 \times 10^{-3}]^T$	0.385
	RK44	$[1, 2.069 \times 10^{-4}, 2.336 \times 10^{-3}, 2.336 \times 10^{-3}]^T$	0.390
	RK55	$[1, 6.952 \times 10^{-4}, -6.158 \times 10^{-5}, 2.336 \times 10^{-3}]^T$	0.443
4	RK33	$[1, 4.833 \times 10^{-4}, 2.336 \times 10^{-5}, -1.438 \times 10^{-4}, 2.637 \times 10^{-4}]^T$	0.431
	RK44	$[1, 1.624 \times 10^{-3}, 2.637 \times 10^{-4}, -2.637 \times 10^{-4}, 2.637 \times 10^{-4}]^T$	0.430
	RK55	$[1, 1.624 \times 10^{-3}, 1.274 \times 10^{-5}, -2.637 \times 10^{-4}, 8.859 \times 10^{-4}]^T$	0.354

Thus far, the investigation has focused exclusively on the linear advection equation. However, for practical applications, non-linear conservation equations will be encountered. Other than the introduction of shock-waves, for which their treatment is still an open question, non-linear equations also introduce aliasing error due to the multiplication of polynomials. This results in a solution that lies beyond the spectral resolution of the grid. Further insight into the origin and effect of order and aliasing was investigated by Kravchenko and Moin.³² Previously, to investigate this problem, a flux function used by Hesthaven and Warburton²³ and Vincent *et al.*⁹ was defined as:

$$f(x; t) = \left((1 - x^2)^5 + 1 \right) u(x, t) \quad (72)$$

However, when applied to a periodic domain $\Omega = [-1, 1]$ the flux function of Eq.(72) is only C^0 continuous. Hence, it is proposed that it would be more suitable to use a flux function defined as:

$$f(x; t) = (\sin(\pi x) + 2)u(x; t) \quad (73)$$

This flux function is strictly linear in u , however the spatial dependence of the flux function, results in the triggering of aliasing error. Therefore, this gives useful insight into GSFR's application to full non-linear problems, without the associated problems of shock formation. To understand the mechanism of production for aliasing error, consider the finite spatial Fourier series of an approximate solution $u(x, t)$:

$$u(x, t) = \sum_{n=-N/2}^{N/2-1} w_n(t) \exp\left(\frac{n\pi i x}{l}\right) \quad (74)$$

where $w_n(t)$ are time dependent Fourier weights, and l is the domain half length. The half length can be used to generalise Eq.(73), such that, together with application of the product rule, one has:

$$\frac{\partial(\sin(\frac{\pi x}{l}) + 2)u}{\partial x} = \left(\sin\left(\frac{\pi x}{l}\right) + 2\right) \frac{\partial u}{\partial x} + \frac{\pi}{l} \cos\left(\frac{\pi x}{l}\right) u \quad (75)$$

By subsequent application of the Fourier series of Eq.(74):

$$\begin{aligned} \frac{\partial(\sin(\frac{\pi x}{l}) + 2)u}{\partial x} = \frac{\pi}{2l} \sum_{n=-N/2}^{N/2-1} w_n(t) & \left(4ni \exp\left(\frac{nx}{l}\right) \right. \\ & + \exp\left(\frac{(n-1)\pi i x}{l}\right) (1+ni) \\ & \left. + \exp\left(\frac{(n+1)\pi i x}{l}\right) (1-ni) \right) \end{aligned} \quad (76)$$

hence, aliasing is injected only by the highest frequency mode and will propagate down through the modes. As opposed to the flux function of Eq.(72), which would cause aliasing error injection at all modes. For the numerical experiment, the domain set up was $\Omega = [-1, 1]$ with periodic boundaries. The method of temporal integration used was low storage RK44, with τ set to be sufficiently small that the temporal integration had a negligible effect on the error. To illustrate the effect on the solution, the domain L^2 energy of the conserved variable is used, defined as:

$$E(t) = \int_{\Omega} u(x, t)^2 dx \quad (77)$$

and the initial condition will be taken as:

$$u(x; t = 0) = \sin(4\pi x) \quad (78)$$

The effect of having a flux function that is C^∞ continuous on Ω is that the periodic boundaries are analogous to solving the same equation on an infinite domain. Hence, the time period of the solution can be found analytically to be $T = 2/\sqrt{3}$. To evaluate the relative performance of correction functions, the L^2 energy error relative to some known value of the L^2 energy is compared for various correction functions. Due to the periodicity of the solution, the error at some time nT , $n \in \mathbb{N}$ may be straightforwardly calculated, *i.e.* analytical energy $E_a(nT) = 1$.

Figure 9 shows just such an error in the L^2 energy, for $p = 3$ with upwinded interfaces. Central differenced interfaces are not shown as, for all correction functions, the scheme had gone unstable within $t = 15T = 30/\sqrt{3}$. This is due to the coupling of the aliasing error to the zero dissipation associated with central difference. The result is that any error introduced into the solution does not become damped and hence instability arises. However, when considering the case of upwinded interfaces, the implicit dissipation in the scheme can be sufficient to stabilise the errors introduced through aliasing. It may also be noted that, from Fig.5, the region of localised peak CFL number lies within a region of low aliasing error and hence correction functions in this region ($\iota_3 \approx 1 \times 10^{-3}$, $\iota_1 \approx 0$) may be good candidates for practical applications. The final investigation will be the application of GSFR to the 3D Euler equations, defined as:

$$\frac{\partial \mathbf{U}}{\partial t} + \nabla \cdot \mathbf{F} = 0 \quad (79)$$

where

$$\mathbf{F} = \left[\mathbf{f}_1 \quad \mathbf{f}_2 \quad \mathbf{f}_3 \right]^T \quad (80)$$

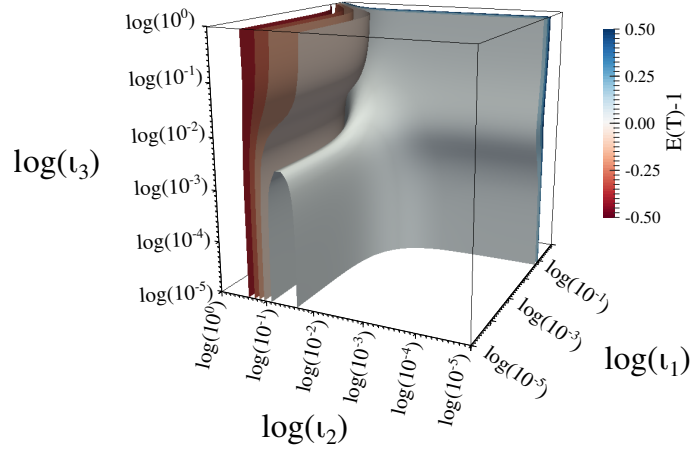


Figure 9: L^2 energy error for FR, $p = 3$, using RK44 temporal integration with CFL = 0.06, for $\alpha = 1$ (upwinded) $t = T = 2/\sqrt{3}$.

$$\mathbf{f}_1 = \begin{bmatrix} \rho u \\ \rho u^2 + p \\ \rho uv \\ \rho uw \\ u(\frac{1}{2}\rho \mathbf{v} \cdot \mathbf{v} + \rho e + p) \end{bmatrix} \quad \mathbf{f}_2 = \begin{bmatrix} \rho v \\ \rho uv \\ \rho v^2 + p \\ \rho vw \\ v(\frac{1}{2}\rho \mathbf{v} \cdot \mathbf{v} + \rho e + p) \end{bmatrix} \quad \mathbf{f}_3 = \begin{bmatrix} \rho w \\ \rho uw \\ \rho vw \\ \rho w^2 + p \\ w(\frac{1}{2}\rho \mathbf{v} \cdot \mathbf{v} + \rho e + p) \end{bmatrix} \quad (81)$$

with $\mathbf{v} = [u, v, w]^T$. The case used to numerically investigate the performance of FR on Euler's Equations is the Isentropic Convecting Vortex (ICV).³³

$$u = u_0 + \frac{\beta(y_c - y)}{2\pi} \exp\left(\frac{1 - r^2}{2}\right) \quad (82)$$

$$v = v_0 + \frac{\beta(x - x_c)}{2\pi} \exp\left(\frac{1 - r^2}{2}\right) \quad (83)$$

$$w = w_0 \quad (84)$$

$$T = 1 - \frac{(\gamma - 1)\beta^2}{8\gamma\pi^2} \exp(1 - r^2) \quad (85)$$

where, β is the vortex strength, x_c and y_c are the grid centre coordinates, γ is the ratio of specific heats, $r = \sqrt{x^2 + y^2}$ and T is temperature. The domain of the solution is taken as $\Omega \in [-10, 10]^3$ with periodic boundaries and the vortex strength $\beta = 5$. For this case the common interface flux calculation used is the Rusanov flux²¹ with characteristic speed from Davis.³⁴ As is shown in Fig.10, all the correction functions taken from the region deemed stable for linear advection, are stable when applied to the ICV. For all correction functions tested, there is a small region, $0 \leq t \leq 2$, where the kinetic energy increases above the initial value, this is likely due to the smoothing of the higher order discontinuities in the solution. The origin of these discontinuities is, although the domain is large, the solution is not strictly C^p continuous on a periodic domain, and the effect of these discontinuities were seen to reduce as the domain is widened. The oscillation that is also seen in all the error plots of Fig.10 is due to the grid affecting integration accuracy and has a frequency that reflects this. The correction functions considered here are: DG; the CFL optimal correction function presented by Vermeire and Vincent;¹⁹ the CFL optimal correction function from Table.1; the correction function found by Vincent *et al.*³⁰ to give best temporal stability this combination of spatial-temporal scheme; and lastly a stable correction function chosen arbitrarily.

It can be clearly seen that DG gives the best performance. Although, it may be expected that the CFL optimal correction function would give best performance, as is shown in Fig.6, this is not the case. The grid used here is sufficient for the solution to be primarily formed of lower wavenumbers, where, as can be seen from the mid section of Fig.6b, DG has the least dissipation. An interesting comparison can be made between the performance of the optimal CFL correction functions for OSFR, ESFR, and GSFR. The OSFR

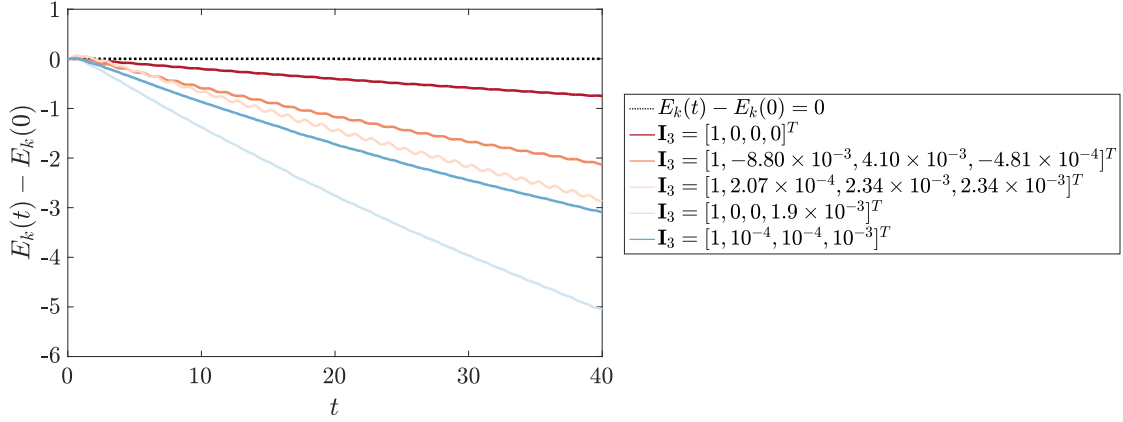


Figure 10: Error in the domain integrated kinetic energy of the ICV for FR, $p = 3$, for various correction functions. Using RK44 temporal integration with $\tau = 10^{-3}$ on $\Omega = [-10, 10]^3$ with $16 \times 16 \times 1$ elements. For the error calculation, $E_k(0)$ was calculated on a $256 \times 256 \times 1$ grid. Finally the convective velocity was taken as $u_0 = v_0 = 1, w_0 = 0$.

case is clearly far more dissipative, from which it could be postulated that the lower order Sobolev terms present in ESFR and GSFR can lead to the cancelling out of unwanted dissipation.

VIII. Conclusions

A new set of correction function has been presented, derived from the idea of energy stability in the broken Sobolev norm. This set of correction functions was shown to contain the OSFR and ESFR correction functions and it was further shown that unique functions could be obtained, that OSFR and ESFR were unable to produce. Hence, the intersection of the sets defining OSFR, ESFR and GSFR can be shown diagrammatically as in Fig.11.

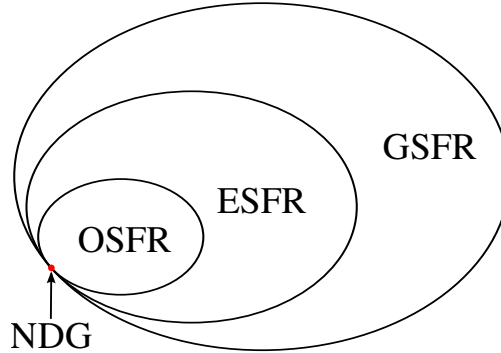


Figure 11: Diagram showing intersection of sets of correction functions.

Study of the linear advection equation, via a von Neumann analysis, was then used to shown that for $p = 3$ a correction function could be found that led to an increase in the CFL number for RK44 temporal integration. It was also demonstrated that this correction function recovers numerically the expected OOA, with GSFR also enabling the recovery of functions from the lower order spaces. A one dimensional linear heterogeneous PDE was proposed to numerically investigate the performance of GSFR when applied to an equation that causes aliasing. The investigation showed that the region of high CFL limit for the case of $p = 3$ was within a stable area of low error. Finally, the solution of Euler's equations on the ICV test case was used to compare the relative performance when applied to fully non-linear PDEs. Of the correction functions tested all remained stable with reasonable performance, however it was found that DG gave the minimal decay in the kinetic energy for this test.

Acknowledgements

The support of the Engineering and Physical Sciences Research Council of the United Kingdom is gratefully acknowledged. The author would like to acknowledge the useful discussions had with Rob Watson and his help in technical editing, language editing, and proofreading.

References

- ¹Chow, F. K. and Moin, P., "A Further Study of Numerical Errors in Large-Eddy Simulations," *Journal of Computational Physics*, Vol. 184, No. 2, 2003, pp. 366–380.
- ²Ghosal, S., "An Analysis of Numerical Errors in Large-Eddy Simulations of Turbulence," *Journal of Computational Physics*, Vol. 125, No. 1, 1996, pp. 187–206.
- ³Lele, S. K., "Compact Finite Difference Schemes With Spectral-Like Resolution," *Journal of Computational Physics*, Vol. 103, No. 1, 1992, pp. 16–42.
- ⁴Pringuey, T. and Cant, R. S., "High Order Schemes on Three-Dimensional General Polyhedral Meshes - Application to The Level Set Method," *Communications in Computational Physics*, Vol. 12, No. 1, 2012, pp. 1–41.
- ⁵Reed, W. H. and Hill, T. R., "Triangular Mesh Methods for the Neutron Transport Equation," *Los Alamos Report LA-UR-73-479*, , No. 836, 1973, pp. 10.
- ⁶Cockburn, B., Karniadakis, G. E., and Shu, C.-W., "The Development of Discontinuous Galerkin Methods," *Discontinuous Galerkin Methods (Newport, RI, 1999)*, Vol. 11, chap. 1, Springer-Verlag, Berlin, 2000, pp. 3–50.
- ⁷Huynh, H. T., "A Flux Reconstruction Approach to High-Order Schemes Including Discontinuous Galerkin Methods," *18th AIAA Computational Fluid Dynamics Conference*, Vol. 2007-4079, 2007, pp. 1–42.
- ⁸Wang, Z. J. and Gao, H., "A unifying lifting collocation penalty formulation including the discontinuous Galerkin, spectral volume/difference methods for conservation laws on mixed grids," *Journal of Computational Physics*, Vol. 228, No. 21, 2009, pp. 8161–8186.
- ⁹Vincent, P. E., Castonguay, P., and Jameson, A., "A New Class of High-Order Energy Stable Flux Reconstruction Schemes," *Journal of Scientific Computing*, Vol. 47, No. 1, 2010, pp. 50–72.
- ¹⁰Huynh, H. T., "A Flux Reconstruction Approach to High-Order Schemes Including Discontinuous Galerkin for Diffusion," *47th AIAA Aerospace Science Meeting*, No. January in Fluid Dynamics and Co-located Conferences, American Institute of Aeronautics and Astronautics, jun 2009, pp. 1–34.
- ¹¹Jameson, A., "A Proof of the Stability of the Spectral Difference Method For All Orders of Accuracy," *Journal of Scientific Computing*, Vol. 45, No. 1-3, 2010, pp. 348–358.
- ¹²Castonguay, P., Williams, D. M., Vincent, P. E., and Jameson, A., "Energy Stable Flux Reconstruction Schemes for Advection-Diffusion Problems," *Computer Methods in Applied Mechanics and Engineering*, Vol. 267, No. 1, 2013, pp. 400–417.
- ¹³Huynh, H. T., "High-Order Methods Including Discontinuous Galerkin by Reconstructions on Triangular Meshes," *49th AIAA Aerospace Sciences Meeting*, No. January, 2011, pp. 1–28.
- ¹⁴Williams, D. M. and Jameson, A., "Energy stable flux reconstruction schemes for advection-diffusion problems on tetrahedra," *Journal of Scientific Computing*, Vol. 59, No. 3, 2014, pp. 721–759.
- ¹⁵Sheshadri, A., *An Analysis of Stability of the Flux Reconstruction Formulation With Applications to Shock Capturing*, Phd thesis, Stanford University, 2016.
- ¹⁶Zwanenburg, P. and Nadarajah, S., "Equivalence between the Energy Stable Flux Reconstruction and Filtered Discontinuous Galerkin Schemes," *Journal of Computational Physics*, Vol. 306, No. 1, feb 2016, pp. 343–369.
- ¹⁷Mengaldo, G., De Grazia, D., Vincent, P. E., and Sherwin, S. J., "On the Connections Between Discontinuous Galerkin and Flux Reconstruction Schemes: Extension to Curvilinear Meshes," *Journal of Scientific Computing*, Vol. 67, No. 3, 2016, pp. 1272–1292.
- ¹⁸Vincent, P. E., Farrington, A. M., Witherden, F. D., and Jameson, A., "An Extended Range of Stable-Symmetric-Conservative Flux Reconstruction Correction Functions," *Computer Methods in Applied Mechanics and Engineering*, Vol. 296, 2015, pp. 248–272.
- ¹⁹Vermeire, B. and Vincent, P., "On the properties of energy stable flux reconstruction schemes for implicit large eddy simulation," *Journal of Computational Physics*, , No. September, 2016.
- ²⁰Courant, R., Friedrichs, K., and Lewy, H., "On the Partial Difference Equations of Mathematical Physics," *IBM Journal*, Vol. 11, No. 2, 1967, pp. 215–234.
- ²¹Rusanov, V., "The Calculation fo the Interaction of Non-Stationary Shock Waves with Barriers," *Zh. Vychisl. Mat. Mat. Fiz.*, Vol. 1, No. 2, 1961, pp. 267–279.
- ²²Toro, E., *Riemann Solvers and Numerical Methods for Fluid Dynamics - A Practical Introduction*, Springer-Verlag Berlin Heidelberg, Dordrecht Berlin Heidelberg London New York, 3rd ed., 2009.
- ²³Hesthaven, J. S. and Warburton, T., *Nodal Discontinuous Galerkin Methods: Algorithms, Analysis, and Applications*, Vol. 54 of *Texts in Applied Mathematics*, Springer New York, New York, NY, 1st ed., 2008.
- ²⁴Bailey, W. N., "On The Product of Two Legendre Polynomials," *Mathematical Proceedings of the Cambridge Philosophical Society*, Vol. 29, No. 02, may 1933, pp. 173–176.
- ²⁵Dougall, J., "On The Product of Two Legendre Polynomials," *Glasgow Mathematical Journal*, Vol. 1, No. 3, 1952, pp. 121–125.
- ²⁶Miller, J., "Formulas for Integrals of Products of Associated Legendre or Laguerre Functions," *Mathematics of Computation*, Vol. 17, No. 81, 1963, pp. 84–84.

- ²⁷Garfinkel, B., “Addition Theorem for a Derivative of a Legendre Polynomial,” *The Astronomical Journal*, Vol. 69, No. 8, 1964, pp. 567–569.
- ²⁸Holdeman, J. T., “Legendre Polynomial Expansions of Hypergeometric Functions with Applications,” *Journal of Mathematical Physics*, Vol. 11, No. 1, 1970, pp. 114–117.
- ²⁹Trojak, W., Watson, R., and Tucker, P. G., “High Order Flux Reconstruction on Stretched and Warped Meshes,” *AIAA SciTech, 55th AIAA Aerospace Sciences Meeting*, Grapevine Texas, 2017, pp. 1–12.
- ³⁰Vincent, P. E., Castonguay, P., and Jameson, A., “Insights From von Neumann Analysis of High-Order Flux Reconstruction Schemes,” *Journal of Computational Physics*, Vol. 230, No. 22, 2011, pp. 8134–8154.
- ³¹Isaacson, E. and Keller, H. B., *Analysis of Numerical Methods*, John Wiley & Sons Ltd., New York, 2nd ed., 1994.
- ³²Kravchenko, A. and Moin, P., “On the Effect of Numerical Errors in Large Eddy Simulations of Turbulent Flows,” *Journal of Computational Physics*, Vol. 131, No. 2, 1997, pp. 310–322.
- ³³Cockburn, B., Johnson, C., Shu, C.-W., and Tadmor, E., *Advanced Numerical Approximation of Nonlinear Hyperbolic Equations*, Springer-Verlag, Berlin Heidelberg, 1st ed., aug 1997.
- ³⁴Davis, S., “Simplified Second-order Godunov-type Methods,” *SIAM Journal on Scientific and Statistical Computing*, Vol. 9, No. 3, 1988, pp. 445–473.

A. L_p Matrix Generation Algorithm

We will detail the basic algorithm for calculating the entries of the matrix \mathbf{L}_p . This is valid for the first $p-2$ rows of \mathbf{L}_p and, as can be seen from Eqs.(47,49,52), the penultimate two rows enforce the boundary conditions of the left correction function.

Algorithm 1 Process for calculating the value of $\mathbf{L}_p[m-1][n]$ for a $\mathbf{I}_p = [\iota_0 \dots \iota_p]$. The method of calculating $I_{i,m,n}$ is given in Algorithm 2.

Require: p, m, n, \mathbf{I}_p
 $L[m-1][n] \leftarrow 0$
for $0 \leq i \leq p$ **do**
 $L[m-1][n] \leftarrow L[m-1][n] + \iota_i I_{i,m,n}$
end for
for $1 \leq i \leq p$ **do**
 $a \leftarrow \frac{(n+i)!(m+i)!}{2^{2i}(i!)^2(n-i)!(m-i)!} (1 - (-1)^{n+m-2i})$
 $L[m-1][n] \leftarrow L[m-1][n] + a \iota_i$
end for
return $L[m-1][n]$

Algorithm 2 Algorithm for calculating the integral of Eq.(44) where $b_i(m, n)$ is defined by Eq.(45).

Require: m, n, k
 $I_{m,n,k} \leftarrow 0$
for $0 \leq i \leq \lfloor \frac{n-m}{2} \rfloor$ **do**
 for $0 \leq j \leq \lfloor \frac{k-m-1}{2} \rfloor$ **do**
 $c \leftarrow \frac{b_i(m,n)b_j(m+1,k)}{n+k-2(m+i+j)} [1 - (-1)^{n+k-2(m+i+j)}]$
 $I_{m,n,k} \leftarrow I_{m,n,k} + c$
 end for
end for
return $I_{m,n,k}$

B. Nomenclature

Roman

a_p	$p!!/p!$
$c(k)$	modified phase velocity at wavenumber k
C^p	p^{th} order differentiability continuous
\mathbf{C}_{+1}	downwind cell FR matrix
\mathbf{C}_0	centre cell FR matrix
\mathbf{C}_{-1}	upwind cell FR matrix
\mathbf{D}	first derivative matrix
E	domain integrated energy of variable
E_k	domain integrated kinetic energy
f	flux variable in physical domain
\mathbf{F}	Array of Euler's equations flux vectors
h_l & h_r	left and right correction functions
\mathbf{H}_p	p^{th} order GSFR correction inverse matrix
g_l & g_r	gradient of the left and right correction functions
J_i	i^{th} cell Jacobian
k	wavenumber
k_{nq}	solution point Nyquist wavenumber, $(p+1)/\delta_j$
\hat{k}	k_{nq} normalised wavenumber, $[0, \pi]$
\mathbf{K}	ESFR correction matrix

l_i	i^{th} Lagrange basis function
\mathbf{L}_p	p^{th} order GSFR correction matrix
\mathbf{M}	polynomial basis mass matrix
p	solution polynomial order
\mathbf{Q}	FR spatial discretisation operator matrix
\mathbf{R}	FR spatial-temporal update matrix
u	conserved variable in the physical domain
\mathbf{V}	polynomial basis matrix
w_i	i^{th} Fourier mode weight

Greek

α	interface upwinding ratio ($\alpha = 1 \Rightarrow$ upwinded, $\alpha = 0.5 \Rightarrow$ central)
δ_j	mesh spacing, $x_j - x_{j-1}$
ϵ_2	domain averaged L^2 norm error
ι	OSFR correction function parameter
ι_i	i^{th} GSFR correction function parameter
\mathbf{I}_p	p^{th} order array of GSFR correction function parameters, $\mathbf{I}_p = [\iota_0 \dots \iota_p]^T$
κ_i	i^{th} ESFR correction parameter
ξ	transformed spatial variable
$\rho(\mathbf{A})$	spectral radius of \mathbf{A}
τ	time step
ψ_i	i^{th} Legendre polynomial of the first kind
Ω	solution domain
Ω_n	n^{th} solution sub-domain
$\hat{\Omega}$	reference sub-domain

Subscript

\bullet_l	variable at left of cell
\bullet_r	variable at right of cell

Superscript

\bullet^I	common value at interface
\bullet^T	vector or matrix transpose
\bullet^δ	discontinuous value
$\hat{\bullet}$	variable transformed to reference domain
$\tilde{\bullet}$	variable transformed to Legendre basis